

REP: Resource-Efficient Prompting for Rehearsal-Free Continual Learning

Sungho Jeon, Xinyue Ma, Kwang In Kim, Myeongjae Jeon

POSTECH

{sunghojeon, xinyuema, kimkin, mj.jeon}@postech.ac.kr

Abstract

Recent rehearsal-free methods, guided by prompts, generally excel in vision-related continual learning (CL) scenarios with continuously drifting data. To be deployable on real-world devices, these methods must maintain high resource efficiency during training. In this paper, we introduce Resource-Efficient Prompting (REP), which targets improving the resource efficiency of prompt-based rehearsal-free methods. Our key focus is on avoiding catastrophic trade-offs with accuracy while trimming computational and memory costs during prompt learning. We achieve this by exploiting swift prompt selection that enhances input data using a carefully provisioned model, and by developing adaptive token merging (AToM) and layer dropping (ALD) algorithms for the prompt updating stage. AToM and ALD perform selective skipping across the data and model-layer dimensions without compromising task-specific features while learning new tasks. We validate REP’s superior resource efficiency over current state-of-the-art ViT- and CNN-based methods through extensive experiments on three image classification datasets.

1. Introduction

Continual learning (CL) trains neural network models on multiple sequential tasks, where each task may include data that diverges from previously encountered data. A crucial challenge for any CL algorithm is to effectively address *catastrophic forgetting* [22]. Severe forgetting occurs when a model rapidly loses previously learned knowledge while adapting to new tasks. The inability to adapt to new tasks not only impairs overall model accuracy but also affects user experiences of AI services in the real world [37].

Moreover, many of today’s AI services are designed for on-device scenarios [10, 18, 39] to securely learn tasks *locally*, without dependence on remote servers over the network. In on-device CL, learning methods must be optimized for *computational* (equivalently, *energy*) and *memory efficiency* requirements. Energy is scarce and can be intermittent in small devices in the wild [1, 14, 17],

yet it is quickly drained by GPU operations during training [21]. Thus, achieving higher computational efficiency while training a new task in CL invariably enhances device durability. In contrast, memory efficiency often acts as a hard constraint. Device memory capacity is typically very limited and unified to operate all CPU and GPU programs. Therefore, a CL task that exhausts all available memory risks system crashes due to out-of-memory errors. As mobile and edge devices adhere to small form factors, it is difficult to dramatically augment battery and memory capacity to address these issues in practice.

In this paper, we present several new techniques for reducing the computational and memory costs of *prompt-based rehearsal-free* methods that leverage frozen, pre-trained vision transformer (ViT) models [15, 29, 34–36]. Prompts are a small set of parameters that progressively learn incoming tasks to combat forgetting. Updates to these compact prompts incur *minimum data writes* without significantly harming the lifespan of device storage, which typically sustains up to 10K writes per location. This makes using prompts a good fit for on-device CL. Moreover, thanks to recent advancements in small-memory ViT models, such as ViT-Ti [30] (5.8M parameters; similar size to ResNet-10), we can always spot powerful ViT models that match the resource efficiency of traditional CNN models under consideration across memory specifications of typical resource-constrained IoT and embedded devices, as shown in Table 1.

To enhance prompt-based CL for resource efficiency, we introduce REP (Resource-Efficient Prompting; Figure 1). REP is built upon our analysis of cost-accuracy trade-offs across the end-to-end learning process, with two key design insights. (1) The *prompt selection* stage, which constructs a prompt subset to augment input or intermediate data, is highly amenable to numerous promising options with fast approximations. (2) In contrast, the *prompt update* stage, which involves forward-backward passes over the backbone model, presents a range of optimizations with vastly different cost-accuracy trade-offs. With these insights, we develop three complementary techniques for both stages that trade minimal accuracy for high resource efficiency: (1) *model downsizing* for prompt selection and (2)

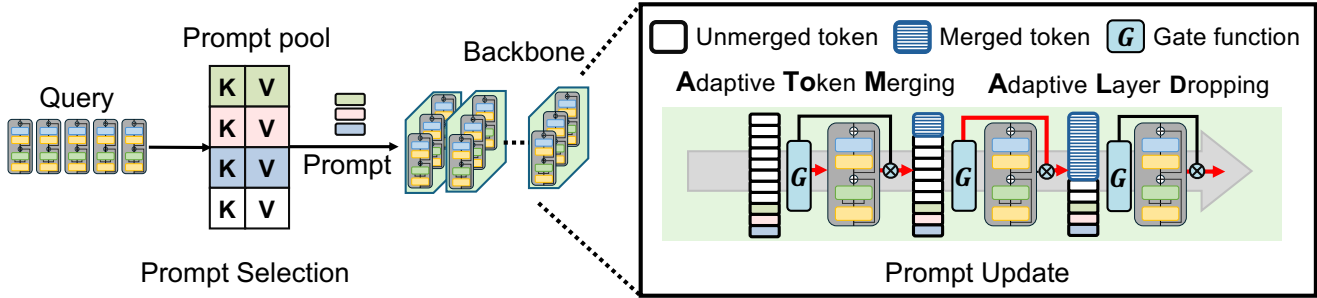


Figure 1. Overview of the proposed resource-efficient prompting (REP) algorithm for rehearsal-free CL. REP calculates query features from input samples using a lightweight model (e.g., ViT-Ti) to swiftly extract prompts from the prompt pool. These prompts are then inserted into a main backbone model (e.g., ViT-L) for training, which prioritizes model accuracy.

Memory Capacity	ViT-Based Methods	CNN-Based Methods
4-8 GB	L2P (ViT-L), DualP (ViT-L) CODA-P (ViT-B)	MEMO (RN26, RN34) BudgetCL (RN101)
1-4 GB	L2P (ViT-B), DualP (ViT-B)	MEMO (RN10, RN18) BudgetCL (RN34)
Up to 1 GB	L2P (ViT-Ti), DualP (ViT-Ti)	BudgetCL (RN10, RN18)

Table 1. ViT- and CNN-based methods with specific backbone models are mapped to the memory capacity they can fit into. DualP is DualPrompt, and CODA-P is CODA-Prompt.

adaptive token merging (AToM) and *adaptive layer dropping* (ALD) for prompt update. In pre-trained ViT models, task-specific knowledge is concentrated in shallow layers, while generalized feature information is spread across all layers [35] (See Figure 2 for our analysis). So, AToM and ALD carry out selective skipping across the data and model-layer dimensions in a “non-uniform” manner to preserve critical task-specific features in the shallow layers. REP provides resource efficiency that aligns with the capabilities of real-world commodity devices including NVIDIA Jetson TX2 and Nano. We evaluate REP across various memory budgets, backbone models, and datasets. Our experiments demonstrate that REP reduces wall-clock training time by 16–47% and lowers memory consumption by 5–33%.

2. Related Work

Class-Incremental Learning. Our work primarily targets class-incremental learning (CIL) among various CL scenarios. In CIL, each incoming task introduces new classes within the same domain during the training phase, while task ID is not at hand during the inference phase [8]. In prior art using CNN backbone networks, *rehearsal-based* methods, which archive and replay representative samples from previous tasks [2, 4, 5, 28], have been a popular choice due to their superior performance [25]. Several recent methods are noteworthy along this line. For instance, BudgetCL [26] and CarM [19] suggest data-driven methods that outper-

form other strategies based on algorithmic optimizations, particularly when training is constrained by compute budgets. MEMO [40] effectively trades memory used to store old samples for saving task-specific model layers. We compare prompt-based methods with some of these methods and confirm better performance under resource constraints.

Continual Learning for the Edge. There has been a notable emphasis on efficient memory and energy usage in on-device learning, particularly in non-CL settings [9, 32, 33]. More recently, a handful of studies have explored extending CL capabilities to edge devices. Hayes and Kanan investigated online CL methods using CNN models tailored for embedded devices and provided valuable algorithmic insights. Similarly, Kwon et al. undertook a comparative analysis of rehearsal vs. regularization methods to uncover the cost-accuracy trade-offs, including storage, compute, and memory requirements. Ma et al. proposed an ML platform called Miro, which dynamically configures key design parameters of CNN-based CL methods to reduce energy costs within the device’s memory capacity. Unfortunately, none of these studies address the specific challenges associated with enabling vision transformers for on-device CL, which stands as a main goal of our research.

Prompting for Continual Learning. The use of prompts, which are explicit instructions or queries given to the model during training or inference, has shown promise in guiding continual learning for vision transformers [13, 15, 29, 34–36]. The general concept is to fine-tune prompts for new tasks while retaining knowledge acquired from previous tasks. L2P [36] and DualPrompt [35] propose prompt-tuning and prefix-tuning approaches, respectively, by selecting applicable prompts from a shared prompt pool. CODA-Prompt [29] introduces attention-conditioned prompts, which inherently facilitate higher prompting capacity. OVOR [13] uses only a single prompt to expedite the prompt selection stage. Our work suggests three complementary prompting techniques that can benefit all the above methods through full or even partial integration.

3. REP: Resource-Efficient Prompting

Prompt-based rehearsal-free CL typically involves two key stages, *prompt selection* and *prompt update*. Figure 1 illustrates an overview of our method REP for making these stages more resource-efficient.

3.1. Prompt Selection

The prompt selection stage operates a neural network model f_{query} to extract representations of input data from a prompt pool P . For a given input x_i^j in task T_i , f_{query} calculates a query feature $q(x_i^j) \in \mathbb{R}^D$ and selects the prompt p^* that maximizes the cosine similarity between the query and pre-trained prompt $p_k \in P$:

$$p^* = \operatorname{argmax}_{p_k \in P} \frac{\langle q(x_i^j), p_k \rangle}{\|q(x_i^j)\| \|p_k\|}. \quad (1)$$

Although f_{query} is used only for model inference, its size, typically equivalent to the primary backbone model, can incur a substantial increase in *computation time* and *memory usage*. This is particularly true when it is implemented with a large transformer model. To mitigate these costs, we propose to adopt a more resource-efficient model $f_{\text{efficient}}$, which has a smaller depth and width than f_{query} .

Simply decreasing one dimension of the model can easily compromise the performance. Thus, we opt for a small pre-trained ViT model (ViT-Ti) as $f_{\text{efficient}}$, which we have found proficient in extracting essential representations without excessively cutting down on depth or width. When $f_{\text{efficient}}$ generates a query feature $q_{\text{efficient}}(x_i^j) \in \mathbb{R}^d$ (where $d \leq D$), we apply a nonlinear random projection ϕ [23] to maintain the integrity of high-dimensional features in the selected prompt $p_{\text{efficient}}^*$, as follows:

$$p_{\text{efficient}}^* = \operatorname{argmax}_{p_k \in P} \frac{\langle \phi(q_{\text{efficient}}(x_i^j)), p_k \rangle}{\|\phi(q_{\text{efficient}}(x_i^j))\| \|p_k\|}. \quad (2)$$

Using ViT-Ti as $f_{\text{efficient}}$ enables a high level of feature overlap with f_{query} . For instance, on Split ImageNet-R, ViT-Ti achieves a prompt overlap of 76.3% on average with ViT-L, the largest f_{query} in consideration, based on canonical-correlation analysis (CCA). This leads to nearly identical accuracy between $f_{\text{efficient}}$ and f_{query} (refer to Table 2).

3.2. Prompt Update

The prompt update stage aims to refine learnable parameters for effective training and task adaptability by combining the softmax cross-entropy loss of the classifier L_{class} and the cosine similarity loss of the prompt L_{prompt} . The combined loss function L is expressed as:

$$L = L_{\text{class}} \left(f_{\text{update}}(x_i^j), y_i^j \right) + L_{\text{prompt}} \left(p^*, q(x_i^j) \right), \quad (3)$$

where f_{update} denotes the backbone model.

3.2.1. Unveiling System-Efficiency Opportunities

Remaining parameters that are not relevant to learnable parameters consist of a number of frozen transformer blocks. Then, are all frozen blocks useful for executing the loss function L , or can we skip some computations to improve resource efficiency?

To answer this question, we explore the feature representations of pre-trained transformer blocks with prompts by analyzing the mean attention distance. Mean attention distance reflects the degree to which an attention head focuses on a specific patch relative to others in the input. This metric is widely used to analyze the layer representation of ViT models during the pre-training process [7, 27]. In our study, we re-purpose this concept to examine the behavior of frozen layers during data drift. For a given head in an attention layer within frozen blocks, let (x_0, y_0) denote the position of a query patch, and (x_i, y_i) denote the positions of patches it attends to, with attention weights a_i . The distance d_i —typically defined as the Euclidean or pixel distance—is calculated as $d_i = (x_i - x_0)^2 + (y_i - y_0)^2$. We then calculate the weighted mean distance as $\frac{\sum_i a_i \cdot d_i}{\sum_i a_i}$.

From a continual learning perspective, lower distances indicate a more localized attention pattern, thereby capturing “task-specific” features. Conversely, higher distances reflect a more global attention pattern, aligning with the extraction of more general, “task-agnostic” features. We measure mean attention distances along two dimensions: by layer ID and by attention head. Figure 2 shows these results when adapting to the first task of Split ImageNet-R.

In Figure 2(a), we present analysis results for the pre-trained layer ID using L2P with ViT-L. The lower layers exhibit highly dispersed attention distances, indicating that they simultaneously capture task-specific and task-agnostic information. However, as we examine deeper layers, these distances become increasingly concentrated at higher values, indicating that deeper layers specialize in capturing task-agnostic information. Taking a closer look at attention heads in a few selected layers in Figure 2(b), we observe that attention distances across the heads vary more widely in shallow layers than in deeper layers. Moreover, the lower distances observed in early heads of these shallow layers suggest that the learnable prompts integrated into the model effectively capture task-specific information. This behavior allows the model to retain task-relevant features while progressively specializing deeper layers for more generalized representations.

Similar behavior is observed when using DualPrompt with ViT-B in Fig. 2(c). Unlike L2P, DualPrompt integrates prompts directly into the input sequence before the attention layer of each transformer block, rather than only into the first block. This suggests that the feature representations of the pre-trained model, which balance local and global information, may not be greatly affected by the prompt method

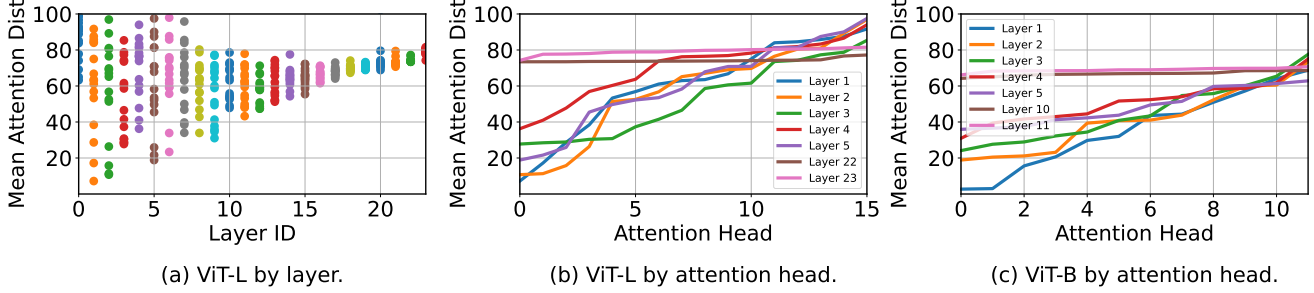


Figure 2. Mean attention distances for frozen blocks along (a) layer IDs and (b/c) attention heads. We run the first task of Split ImageNet-R. (a/b) L2P with ViT-L, and (c) DualPrompt with ViT-B.

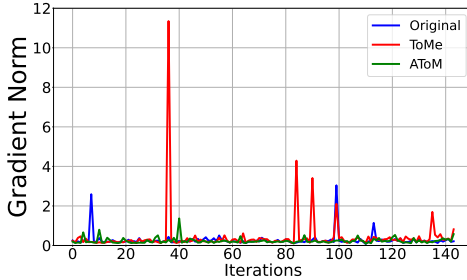


Figure 3. The gradient norm for the prompt when applying conventional token merging (ToMe) vs AToM. L2P with ViT-L runs on Split ImageNet-R.

in use.

Next, we explain how we bring these insights into practice through two compute-skipping techniques.

3.2.2. Adaptive Token Merging (AToM)

We first consider the data-efficient compute-skipping method via token merging. Conventional token merging (ToMe) [3] reduces the number of tokens by *uniformly* merging n redundant tokens per layer, controlled by a fixed scheduler r . The scheduler function $r(l) \rightarrow n$ is applied to each layer l , and according to [3], it merges all tokens, including selected prompts. However, insights from Figure 2 and our additional analysis highlight two major problems.

First, there is a *loss of task-specific information*. The prompt tokens in CL carry essential task-specific information. However, ToMe indiscriminately combines these prompt tokens with others, thereby diminishing their intrinsic value. According to our empirical data in Figure 3, this approach can cause gradient explosions in the prompt tokens, even with gradient clipping, leading to learning instability. Second, there is a *lack of layer-specific adaptability*. Conventional token merging does not account for the disparity between shallow and deep layers, treating all layers uniformly. Therefore, there is a risk of excessive loss of valuable information from shallow layers, which are mainly

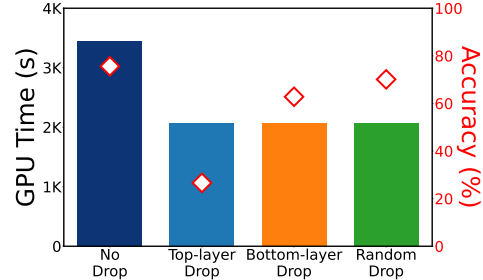


Figure 4. Comparing various layer dropping strategies using L2P with the ViT-L backbone on Split ImageNet-R.

responsible for adaptability to diverse sequential tasks.

Our *adaptive token merging* (AToM; Algorithm 1) addresses the loss of task-specific information by excluding prompt tokens during token merging, thus maintaining their specificity. To enhance task-specific adaptability, AToM uses a new scheduler $r'(l) \rightarrow n'$, which dynamically adjusts the number of tokens to merge based on layer depth, as follows:

$$r'(l) = \min(\delta \times (l - 1), r_{\max}), \quad (4)$$

where l denotes the layer index, δ is the step change in the number of tokens to merge defined as $\frac{r_{\max}}{L-1}$ (with L being the number of layers), and r_{\max} is the maximum number of tokens to merge (by default, $2 \times n$). With this $r'(l)$, merging occurs more frequently in deeper layers than in shallow layers, preserving important task-related representations.

3.2.3. Adaptive Layer Dropping (ALD)

Inspired by insights from Figure 2 and prior work on progressive layer dropping (PLD) [38], we propose *adaptive layer dropping* (ALD; Algorithm 2) with two key features: (1) the dropping schedule considers both temporal and spatial dimensions¹, and (2) it manages to drop layers non-

¹The spatial dimension refers to the different layers of the model. Each layer processes input features at varying levels of abstraction.

Algorithm 1 Adaptive Token Merging (AToM)

Input: Initial set of all tokens T ; Set of prompt tokens P ; Number of model layers L ; Maximum number of tokens to merge r_{\max}

Initialize: $T'_{\text{final}} \leftarrow T$;

```

1: for  $l \in \{1, 2, \dots, L\}$  do
2:    $T_{\text{attn}} \leftarrow \text{MSA}(T'_{\text{final}})$ 
3:    $T_{\text{eligible}} \leftarrow T_{\text{attn}} \setminus P$ 
4:    $\delta \leftarrow \frac{r_{\max}}{L-1}$ 
5:    $n' \leftarrow \min(\delta \times (l-1), r_{\max})$ 
6:    $T'_{\text{merged}} \leftarrow \text{Merge}(T_{\text{eligible}}, n')$ 
7:    $T_{\text{concat}} \leftarrow \text{Concat}(T'_{\text{merged}}, P)$ 
8:    $T'_{\text{final}} \leftarrow \text{MLP}(T_{\text{concat}}, l)$ 
9: end for
10: return  $T'_{\text{final}}$ 

```

uniformly to preserve critical task-specific features in shallower layers. On the contrary, PLD only considers the temporal aspect and does not differentiate between layers when dropping. This results in poorer performance compared to ALD, as shown in Table 3.

To strengthen our claim, we conduct a simple experiment that drops 25% of layers from various positions. We compare their training wall-clock GPU time and final average accuracy in Figure 4 (See Section 4 for details on these metrics), using L2P with the ViT-L backbone on Split ImageNet-R. Specifically, Top-layer Drop and Bottom-layer Drop *statically* drop the first and last 25% of layers, respectively, while Random Drop *randomly* skips 25% of layers across the network. For comparison, we also include No Drop, which performs no layer dropping. Although all these naïve strategies incur accuracy loss, Bottom-layer Drop performs significantly worse than the others. Also, it appears undesirable to bypass only deep layers, even though these layers mainly capture general, task-agnostic features. While Random Drop most closely approaches No Drop’s accuracy, its uniform layer dropping still sacrifices some accuracy. This is why our method ALD carefully accounts for each layer’s spatial aspect in a non-uniform manner to minimize the impact on accuracy.

ALD prioritizes retaining shallow layers that contain richer information essential for model performance, especially after token merging. Thus, instead of operating on its own schedule parameters, ALD leverages feedback from AToM, specifically the count of merged tokens at each layer, to guide layer dropping decisions. The layer-keeping probability $\theta_{t,l}$ is defined as:

$$\theta_{t,l} = (\alpha(l) \times ((1 - \bar{\theta}) \exp(-\gamma \cdot t) + \bar{\theta})) , \quad (5)$$

where $\theta_{t,l}$ is the probability of keeping layer l at time step t , $\bar{\theta}$ is the minimum probability, γ controls the rate of decay,

Algorithm 2 Adaptive Layer Dropping (ALD)

Input: Input tensor X ; Keep ratio of layer $\theta_{t,l}$; Number of layers L ; Minimum ratio $\bar{\theta}$; Decay rate γ ; Spatial threshold τ ; Adjustment factor α

```

1: for  $l \in \{1, 2, \dots, L\}$  do
2:   if  $(n(l) - n'(l)) > \tau$  then
3:      $\alpha(l) \leftarrow \alpha$ 
4:   else
5:      $\alpha(l) \leftarrow 1$ 
6:   end if
7:    $\theta_{t,l} \leftarrow \alpha(l) \times ((1 - \bar{\theta}) \exp(-\gamma \cdot t) + \bar{\theta})$ 
8:   if Bernoulli( $\theta_{t,l}$ ) = 1 then
9:      $X_{\text{out}} \leftarrow \text{Exec}(l, X_{\text{out}})$ 
10:  else
11:     $X_{\text{out}} \leftarrow X_{\text{out}}$ 
12:  end if
13: end for
14: return  $X_{\text{out}}$ 

```

and $\alpha(l)$ is the adjustment factor for layer l defined as:

$$\alpha(l) = \begin{cases} \alpha & \text{if } (n(l) - n'(l)) \geq \tau \\ 1 & \text{if } (n(l) - n'(l)) < \tau. \end{cases} \quad (6)$$

$\alpha(l)$ reflects the extent of token merging performed by AToM in layer l . $n(l)$ represents the original number of tokens, and $n'(l)$ is the number of tokens remaining after merging. When the number of merged tokens surpasses the threshold τ , ALD adjusts the layer-dropping probability based on α . Since deeper layers tend to merge more tokens with AToM, ALD is more likely to exceed τ in deeper layers and drop more aggressively. These parameters should be tuned to balance between efficiency and the need to process the nuanced information contained in the merged tokens. We set α to 0.9, and τ to 16 for ViT-L, 12 for ViT-B, respectively.

One might contemplate exploiting stochastic depth [12], which gradually increases dropping probabilities for deeper layers without a temporal schedule. We compared ALD and stochastic depth and found that ALD generally offers 1.8–3.3% higher accuracy. This may be attributed to early training iterations after task insertion, which play a critical role in stabilizing training losses [21].

Resource Efficiency. REP triggers AToM and ALD for each task insertion to optimize both time and memory usage. Much like our prompt selection optimization, AToM consistently enhances time and memory efficiency. In contrast, ALD solely contributes to reducing time costs because it operates layer-keeping probability $\theta_{t,l}$ starting at 1.0, *i.e.*, no layer dropping, which necessitates traversing full layers.

4. Experiments of REP

We focus on the popular disjoint-CIL setup, where tasks consist of distinct sets of non-overlapping classes and samples from old classes are not given in future tasks [4, 8, 28].

Throughout this section, we will first describe the superiority of ViT-based prompting methods. However, it is important to note that the best-performing method is not fixed and can dynamically change depending on the device memory budget at hand. Therefore, to enhance prompt-based CL for better resource efficiency, we need *adaptive techniques tailored to any backbone* that function regardless of the specific learning method in use. REP is designed for this purpose, and we will evaluate this aspect in detail.

Data Generation. To organize task streams, we use three image classification datasets: CIFAR-100 (100 classes) [16], ImageNet-R (200 classes) [11], and PlantDisease (38 classes) [24]. Out of these datasets, ImageNet-R is known for exhibiting much higher intra-class variability among images and an uneven class-size distribution. We divide CIFAR-100 and ImageNet-R into 10 tasks to create **Split CIFAR-100** (i.e., 10 classes per task) and **Split ImageNet-R** (i.e., 20 classes per task), respectively [29, 35, 36]. For PlantDisease, we drop 3 plant disease classes with very few images and organize the remaining 35 classes into 7 tasks to create **Split PlantDisease** (i.e., 5 classes per task).

Methods. We implement **L2P** [36], **DualPrompt** [35], and **CODA-Prompt** [29] as representative ViT-based prompting methods using PyTorch. L2P and DualPrompt select suitable prompts via inference, similar to [31], while CODA-Prompt employs a strategy for adaptively optimizing prompts *without* prompt selection, similar to [13]. These methods capitalize on ImageNet pre-trained models as backbones: ViT-L (307M), ViT-B (86M), and ViT-Ti (5.8M)—ViT-Ti is *one of the smallest vision transformer models* to our knowledge. We categorize the prompt-based methods into three groups based on their memory consumption, as detailed in Table 1, to reflect diverse device memory capacities.

To demonstrate the effectiveness of prompting methods, we also incorporate two state-of-the-art CNN-based methods, **BudgetCL** [6] and **MEMO** [40]. Both BudgetCL and MEMO improve model accuracy by leveraging spare memory to store and replay past samples, with MEMO additionally storing model checkpoints from history. These methods also utilize ImageNet pre-trained models as backbones: ResNet-10 (RN10; 5M), ResNet-18 (RN18; 11M), ResNet-26 (RN26; 14M), ResNet-34 (RN34; 22M), and ResNet-101 (RN101; 43M) models. For fair comparisons, we similarly group methods based on their memory usage. We refer readers to supplementary materials for detailed settings of all methods mentioned above.

Hardware and Metrics. Given that not all CL methods are currently feasible on small devices due to memory limitations, we use NVIDIA RTX 3090 Ti as a reference GPU and use the wall-clock time required to complete all tasks—Training wall-clock time correlates *linearly* with energy usage [21]. In supplementary materials, we evaluate our memory-efficient method directly on NVIDIA Jetson TX2, although it is applicable beyond this specific device. We also report the final average accuracy by averaging the accuracy of all classes after the last task training, and the forgetting metric [5, 29], which assesses the decline in task accuracy averaged over all tasks.

4.1. Preliminary Empirical Study

We first uncover the *energy-accuracy trade-offs* to highlight the impact of each baseline method on the accuracy gained relative to its training cost. Figure 5 visually represents the comparison results across device memory capacities and datasets. In each graph, the x-axis indicates wall-clock time, which corresponds to energy cost (lower is better), while the y-axis indicates final average accuracy (higher is better). Thus, a more cost-effective method appears closer to the upper-left corner of the graph. Overall, ViT-based methods outperform CNN-based methods by a large margin, achieving 26–36% higher accuracy with 45–90% less time and energy spent under the same memory budget. We elaborate on two key characteristics that explain these results:

- **Performance scaling.** ViT-based methods scale well, with larger backbone networks overall yielding higher accuracy. In contrast, CNN-based methods scale poorly with increased backbone size. Specifically, on Split ImageNet-R, a more challenging dataset, MEMO/RN34 is only 2.95% better than MEMO/RN18, despite being around twice larger. On Split CIFAR-100, increasing the backbone size yields only limited gains.

- **Memory efficiency.** CNN-based methods are often considered more memory-efficient because they use backbones a magnitude smaller than ViT models. Thus, it is commonly believed that ample memory can be allocated to replay samples or past model checkpoints [40], which help improve model performance. However, in CL, which involves typical training iterations, a substantial amount of memory must be allocated for feature maps [20], leaving little room for memory buffers. For instance, for a device memory range of 1–4GB in Table 1, the backbone of MEMO/RN18 consumes only 43MB of memory (6.5% of ViT-L), but feature maps occupy as much as 1.7GB (more than ViT-based methods). This causes MEMO/RN18 to be short on memory for the replay buffer, dramatically degrading model accuracy, as observed in Figure 5.

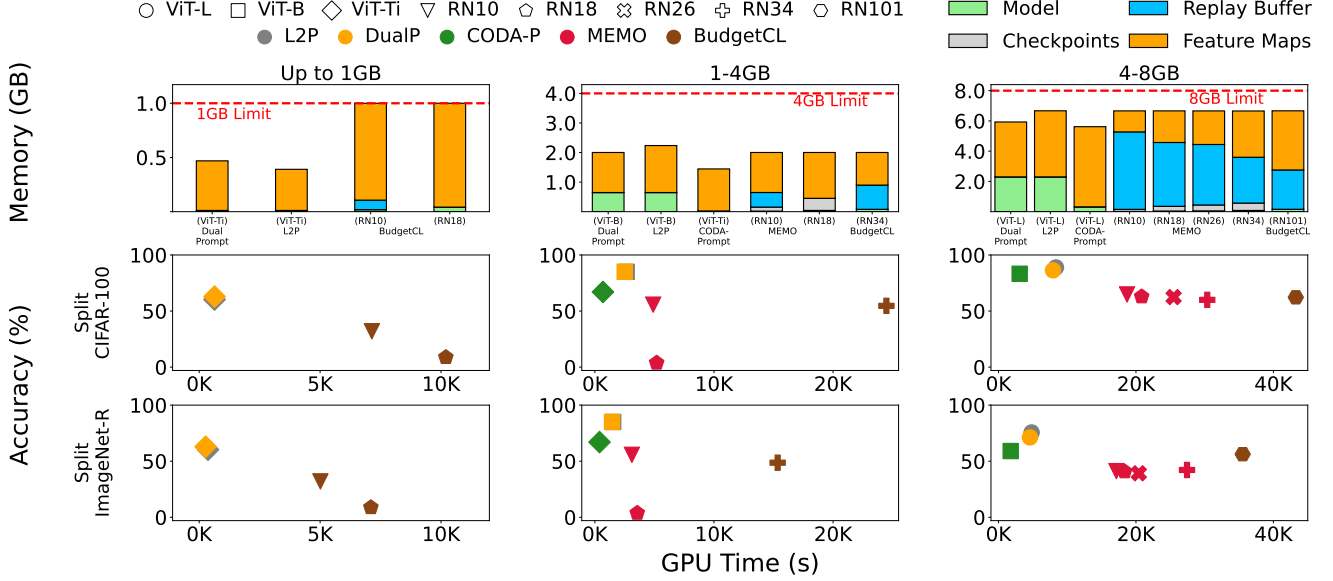


Figure 5. Energy-accuracy trade-offs of various ViT- and CNN-based methods over three different memory budgets: up to 1GB, 1-4GB, and 4-8GB. The memory breakdown of each method is on the first row. Experiments on Split CIFAR-100 and Split ImageNet-R are on the second and third row, respectively. ViT-based methods consistently outperform CNN-based methods.

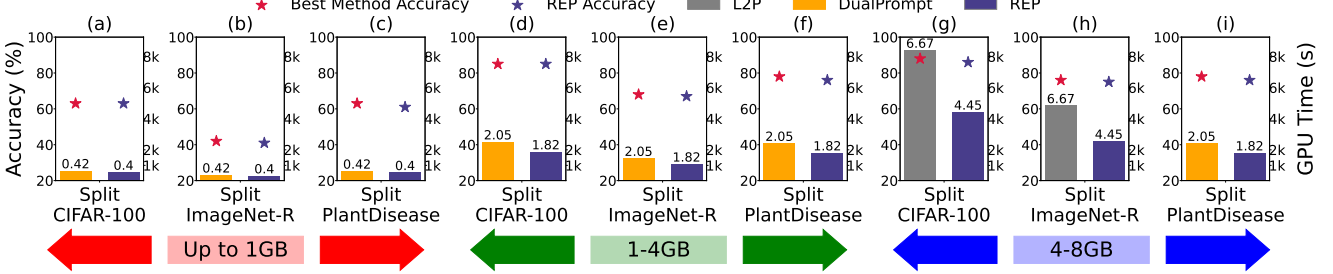


Figure 6. REP over the best methods across various memory budgets and datasets.

4.2. REP on Best-Performing Methods

Next, in each graph in Figure 6, we demonstrate the efficacy of REP when applied to the best-performing CL method for each combination of memory budget and dataset observed in Figure 5. Accuracy is indicated by stars (\star), while GPU wall-clock time is indicated by bars (\blacksquare). The memory usage in GB is noted on top of the bars. Please refer to the supplementary document for the full results of all datasets.

Resource Efficiency. The best-performing baselines optimized with REP demand significantly smaller amounts of system resources. Specifically, REP reduces memory consumption by 33% for L2P/ViT-L, 11% for DualPrompt/ViT-B, and 5% for DualPrompt/ViT-Ti. Despite the frozen backbone not requiring gradients for parameter updates, it still performs the backward pass to calculate classification and prompt losses for updating learnable parameters. Therefore, all intermediate data are stored in memory, similar to

training a non-frozen model. This memory usage is reduced by applying AToM and ALD. In addition, REP exhibits a 16–47% reduction in GPU wall-clock time compared to competing methods, leading to great energy savings.

Accuracy. L2P, DualPrompt, and CODA-Prompt were initially evaluated using only ViT-B backbone, focusing primarily on accuracy in their original studies. In comparison, our evaluation extends these methods across diverse backbones while taking into account their energy-accuracy trade-offs in on-device CL across various memory constraints. When augmented with our techniques, these methods show significant improvements in resource efficiency with minimal accuracy loss across all memory budgets: 0.09–1.90% for Split PlantDisease, 0.03–1.07% for Split CIFAR-100, and 0.26–0.86% for Split ImageNet-R. Especially for the Split PlantDiseases, REP with DualPrompt/ViT-B performed best under both 1–4GB and 4–8GB budgets.

Ablated components	Acc. (\uparrow)	Fgt. (\downarrow)	GPU Time (s)	Mem. (GB)
REP (ours)	75.34 \pm 0.86	3.58 \pm 0.29	2542.43	4.45
(1) $f_{\text{efficient}}$	74.79 \pm 0.78	4.04 \pm 0.80	3698.78	5.53
(2) AToM	74.91 \pm 0.77	3.47 \pm 0.84	4442.04	5.60
(3) ALD	74.53 \pm 0.78	3.63 \pm 0.67	4243.97	6.67
(4) $f_{\text{efficient}}$ + AToM	74.15 \pm 0.82	4.03 \pm 0.76	2861.35	4.46
(5) $f_{\text{efficient}}$ + ALD	74.52 \pm 0.43	3.43 \pm 0.54	3206.74	5.51
(6) AToM + ALD	74.57 \pm 0.37	2.56 \pm 0.52	3448.76	4.77

Table 2. Ablating REP’s components. They contribute to resource efficiency and accuracy.

	Acc. (\uparrow)	Fgt. (\downarrow)	GPU Time (s)	Mem. (GB)
REP (ours)	75.34 \pm 0.86	3.58 \pm 0.29	2542.43	4.45
(1) w/ ToMe	70.19 \pm 0.74	2.63 \pm 0.92	2917.84	3.74
(2) w/ PLD	73.33 \pm 0.71	3.88 \pm 0.69	2741.90	4.46

Table 3. Accuracy of using traditional token merging (ToMe) or layer dropping (PLD) instead of our adaptive algorithms.

n (w/ $\theta=0.5$)	Acc. (\uparrow)	Fgt. (\downarrow)	GPU Time (s)	Mem. (GB)
2	76.16 \pm 0.74	3.54 \pm 0.68	2808.43	5.48
4	75.32 \pm 0.32	3.33 \pm 0.45	2714.04	5.16
8	75.34 \pm 0.86	3.58 \pm 0.29	2542.43	4.45
θ (w/ n=8)	Acc. (\uparrow)	Fgt. (\downarrow)	GPU Time (s)	Mem. (GB)
0.25	73.18 \pm 0.55	4.03 \pm 0.49	2362.07	4.45
0.50	75.34 \pm 0.86	3.58 \pm 0.29	2542.43	4.45
0.75	74.44 \pm 0.60	3.49 \pm 0.53	2861.35	4.45

Table 4. REP over different # of merged tokens (n) and % of keep ratio (θ). We use $n = 8$ and $\theta = 0.5$ as default values.

4.3. Ablation and Additional Study

We validate our proposed techniques and algorithm designs along with the chosen hyperparameters. The study here primarily uses the ViT-L backbone on Split ImageNet-R, where L2P is the best non-optimized method.

Component Ablation. In Table 2, we ablate REP’s components to assess their contributions to resource efficiency. Each component plays a key role in reducing memory and compute time, with ALD affecting compute time only, as expected. Notably, AToM substantially optimizes both resource usages.

Algorithm Validation. Token merging (ToMe) [3] and progressive layer dropping (PLD) [38] are specifically designed to accelerate traditional transformer-based model training. To validate the importance of incorporating our adaptive techniques instead in CL, we evaluate how REP performs in case AToM and ALD are replaced with ToMe and PLD, respectively. The results are presented in Table 3. Although applying ToMe or PLD improves system efficiency over L2P, it results in an accuracy loss of 5.15% or 2.01%, respectively, compared to using our techniques. This indicates that ToMe and PLD are less desirable for achieving our goal, i.e., enhancing system efficiency with-

Method	Acc. (\uparrow)	Fgt. (\downarrow)	GPU Time (s)	Mem. (GB)
REP (ours)	75.34 \pm 0.16	3.58 \pm 0.29	2542.43	4.45
L2P	61.57 \pm 0.66	9.73 \pm 0.47	1609.88	14.20
DualPrompt	68.13 \pm 0.49	4.68 \pm 0.20	1507.42	12.30
CODA-Prompt	75.45 \pm 0.56	1.64 \pm 0.10	1853.54	18.83

Table 5. Results on Split ImageNet-R, with ViT-B as the backbone model (following the original setups).

out compromising accuracy.

AToM and ALD Intensity. Table 4 shows the effects of varying intensities of AToM and ALD, focusing on the number of merged tokens (n) in AToM and the keep ratio (θ) in ALD. AToM appears to maintain stable accuracy even as more tokens are merged. In contrast, for ALD, a lower keep ratio improves system efficiency by reducing iteration time and memory usage, but it can markedly impair model accuracy if the ratio is too low. Overall, when used with caution, AToM and ALD can effectively balance system efficiency and accuracy.

Longer Task Sequence. We examine how REP performs on a longer task sequence of 20 tasks. A longer task sequence represents a more challenging scenario, where performance drop as the number of tasks increases can become more pronounced. We observe that REP consistently preserves model accuracy (from 72.77 \pm 0.19 in L2P to 72.58 \pm 0.59 in REP) while improving resource efficiency by 47.3% and 33%, respectively.

Competing Methods with Original Setups. For L2P, DualPrompt, and CODA-Prompt, we used the hyperparameters of the original papers, except for the number of iterations per task and batch size. In particular, smaller batch sizes must be adopted to fit into on-device memory constraints. Nonetheless, we present the results of three competing methods on Split ImageNet-R using their original hyperparameters in Table 5. Despite using the ViT-B backbone, they consume significantly more memory than REP due to their large batch sizes.

5. Discussion

Since our study focuses on scenarios wherein a sequence of tasks is presented within learning environments, our method does not determine the *curriculum* of learning. In general, actively selecting such curricula could enhance the final average accuracy, motivating future work to extend our method for curriculum-based continual learning. Moreover, although using replay buffer may not be feasible in real-world scenarios due to data privacy concerns, on-device CL is already viewed as a privacy-preserving approach, making rehearsal-based REP a promising direction.

References

[1] Saad Ahmed, Bashima Islam, Kasim Sinan Yildirim, Marco Zimmerling, Przemysław Pawelczak, Muhammad Hamad Alizai, Brandon Lucia, Luca Mottola, Jacob Sorber, and Josiah Hester. The Internet of Batteryless Things. *ACM*, 67(3):64–73, 2024. 1

[2] Jihwan Bang, Heesu Kim, YoungJoon Yoo, Jung-Woo Ha, and Jonghyun Choi. Rainbow Memory: Continual Learning with a Memory of Diverse Samples. In *CVPR*, 2021. 2

[3] Daniel Bolya, Cheng-Yang Fu, Xiaoliang Dai, Peizhao Zhang, Christoph Feichtenhofer, and Judy Hoffman. Token Merging: Your ViT But Faster. In *ICLR*, 2023. 4, 8

[4] Francisco M. Castro, Manuel J. Marin-Jimenez, Nicolas Guil, Cordelia Schmid, and Karteek Alahari. End-to-End Incremental Learning. In *ECCV*, 2018. 2, 6

[5] Arslan Chaudhry, Puneet K. Dokania, Thalaiyasingam Ajanthan, and Philip H. S. Torr. Riemannian Walk for Incremental Learning: Understanding Forgetting and Intransigence. In *ECCV*, 2018. 2, 6

[6] Arslan Chaudhry, Marcus Rohrbach, Mohamed Elhoseiny, Thalaiyasingam Ajanthan, Puneet K. Dokania, Philip HS Torr, and Marc’Aurelio Ranzato. On Tiny Episodic Memories in Continual Learning. *arXiv:1902.10486*, 2019. 6

[7] Alexey Dosovitskiy, Lucas Beyer, Alexander Kolesnikov, Dirk Weissenborn, Xiaohua Zhai, Thomas Unterthiner, Mostafa Dehghani, Matthias Minderer, Georg Heigold, Sylvain Gelly, Jakob Uszkoreit, and Neil Houlsby. An Image is Worth 16x16 Words: Transformers for Image Recognition at Scale. In *ICLR*, 2021. 3

[8] Alexander Gepperth and Barbara Hammer. Incremental Learning Algorithms and Applications. In *ESANN*, 2016. 2, 6

[9] In Gim and JeongGil Ko. Memory-Efficient DNN Training on Mobile Devices. In *MobiSys*, 2022. 2

[10] Tyler L Hayes and Christopher Kanan. Online Continual Learning for Embedded Devices. In *CoLLAs*, 2022. 1, 2

[11] Dan Hendrycks, Steven Basart, Norman Mu, Saurav Kadavath, Frank Wang, Evan Dorundo, Rahul Desai, Tyler Zhu, Samyak Parajuli, Mike Guo, Dawn Song, Jacob Steinhardt, and Justin Gilmer. The Many Faces of Robustness: A Critical Analysis of Out-of-Distribution Generalization. In *ICCV*, 2021. 6

[12] Gao Huang, Yu Sun, Zhuang Liu, Daniel Sedra, and Kilian Q Weinberger. Deep Networks with Stochastic Depth. In *ECCV*, 2016. 5

[13] Wei-Cheng Huang, Chun-Fu Chen, and Hsiang Hsu. OVOR: OnePrompt with Virtual Outlier Regularization for Rehearsal-Free Class-Incremental Learning. In *ICLR*, 2024. 2, 6

[14] Seunghyeok Jeon, Yonghun Choi, Yeonwoo Cho, and Ho-jung Cha. HarvNet: Resource-Optimized Operation of Multi-Exit Deep Neural Networks on Energy Harvesting Devices. In *MobiSys*, 2023. 1

[15] Dahuin Jung, Dongyo Han, Jihwan Bang, and Hwanjun Song. Generating Instance-level Prompts for Rehearsal-free Continual Learning. In *ICCV*, 2023. 1, 2

[16] Alex Krizhevsky and Geoffrey Hinton. Learning Multiple Layers of Features from Tiny Images. *Master’s thesis, Department of Computer Science, University of Toronto*, 2009. 6

[17] Jaeheon Kwak, Sunjae Lee, Dae R Jeong, Arjun Kumar, Dongjae Shin, Ilju Kim, Donghwa Shin, Kilho Lee, Jinkyu Lee, and Insik Shin. MixMax: Leveraging Heterogeneous Batteries to Alleviate Low Battery Experience for Mobile Users. In *MobiSys*, 2023. 1

[18] Young D Kwon, Jagmohan Chauhan, Abhishek Kumar, Pan Hui HKUST, and Cecilia Mascolo. Exploring System Performance of Continual Learning for Mobile and Embedded Sensing Applications. In *IEEE/ACM SEC*, 2021. 1, 2

[19] Soobee Lee, Minindu Weerakoon, Jonghyun Choi, Minjia Zhang, Di Wang, and Myeongjae Jeon. CarM: Hierarchical Episodic Memory for Continual Learning. In *DAC*, 2022. 2

[20] Gangmuk Lim, Jeongseob Ahn, Wencong Xiao, Youngjin Kwon, and Myeongjae Jeon. Zico: Efficient GPU Memory Sharing for Concurrent DNN Training. In *USENIX ATC*, 2021. 6

[21] Xinyue Ma, Suyeon Jeong, Minjia Zhang, Di Wang, Jonghyun Choi, and Myeongjae Jeon. Cost-effective On-device Continual Learning over Memory Hierarchy with Miro. In *MobiCom*, 2023. 1, 2, 5, 6

[22] Michael McCloskey and Neal J. Cohen. Catastrophic Interference in Connectionist Networks: The Sequential Learning Problem. In *Psychol. Learn. Motiv. - Adv. Res. Theory*, 1989. 1

[23] Mark D McDonnell, Dong Gong, Amin Parvaneh, Ehsan Abbasnejad, and Anton van den Hengel. Random Projection in Deep Neural Networks. In *NeurIPS*, 2024. 3

[24] Sharada Prasanna Mohanty, David Hughes, and Marcel Salathe. Using Deep Learning for Image-Based Plant Disease Detection. *arXiv:1604.0316*, 2016. 6

[25] Ameya Prabhu, Philip HS Torr, and Puneet K Dokania. GDumb: A Simple Approach that Questions Our Progress in Continual Learning. In *ECCV*, 2020. 2

[26] Ameya Prabhu, Hasan Abed Al Kader Hammoud, Puneet K. Dokania, Philip H.S. Torr, Ser-Nam Lim, Bernard Ghanem, and Adel Bibi. Computationally Budgeted Continual Learning: What Does Matter? In *CVPR*, 2023. 2

[27] Maithra Raghu, Thomas Unterthiner, Simon Kornblith, Chiyuan Zhang, and Alexey Dosovitskiy. Do Vision Transformers See Like Convolutional Neural Networks? In *NeurIPS*, 2021. 3

[28] Sylvestre-Alvise Rebuffi, Alexander Kolesnikov, Georg Sperl, and Christoph H. Lampert. iCaRL: Incremental Classifier and Representation Learning. In *CVPR*, 2017. 2, 6

[29] James Seale Smith, Leonid Karlinsky, Vyshnavi Gutta, Paola Cascante-Bonilla, Donghyun Kim, Assaf Arbelle, Rameswar Panda, Rogerio Feris, and Zsolt Kira. CODA-Prompt: COntinual Decomposed Attention-based Prompting for Rehearsal-Free Continual Learning. In *CVPR*, 2023. 1, 2, 6

[30] Andreas Peter Steiner, Alexander Kolesnikov, Xiaohua Zhai, Ross Wightman, Jakob Uszkoreit, and Lucas Beyer. How to train your ViT? Data, Augmentation, and Regularization in Vision Transformers. *TMLR*, 2022. 1

- [31] Liyuan Wang, Jingyi Xie, Xingxing Zhang, Mingyi Huang, Hang Su, and Jun Zhu. Hierarchical Decomposition of Prompt-Based Continual Learning: Rethinking Obscured Sub-optimality. In *NeurIPS*, 2023. [6](#)
- [32] Qipeng Wang, Mengwei Xu, Chao Jin, Xinran Dong, Jinliang Yuan, Xin Jin, Gang Huang, Yunxin Liu, and Xuanzhe Liu. Melon: Breaking the Memory Wall for Resource-Efficient on-Device Machine Learning. In *MobiSys*, 2022. [2](#)
- [33] Yue Wang, Ziyu Jiang, Xiaohan Chen, Pengfei Xu, Yang Zhao, Yingyan Lin, and Zhangyang Wang. E2-Train: Training State-of-the-art CNNs with Over 80% Energy Savings. In *NeurIPS*, 2019. [2](#)
- [34] Yabin Wang, Zhiwu Huang, and Xiaopeng Hong. S-Prompts Learning with Pre-trained Transformers: An Occam’s Razor for Domain Incremental Learning. In *NeurIPS*, 2022. [1](#), [2](#)
- [35] Zifeng Wang, Zizhao Zhang, Sayna Ebrahimi, Ruoxi Sun, Han Zhang, Chen-Yu Lee, Xiaoqi Ren, Guolong Su, Vincent Perot, Jennifer Dy, and Tomas Pfister. DualPrompt: Complementary Prompting for Rehearsal-Free Continual Learning. In *ECCV*, 2022. [2](#), [6](#)
- [36] Zifeng Wang, Zizhao Zhang, Chen-Yu Lee, Han Zhang, Ruoxi Sun, Xiaoqi Ren, Guolong Su, Vincent Perot, Jennifer Dy, and Tomas Pfister. Learning To Prompt for Continual Learning. In *CVPR*, 2022. [1](#), [2](#), [6](#)
- [37] Dianlei Xu, Tong Li, Yong Li, Xiang Su, Sasu Tarkoma, Tao Jiang, Jon Crowcroft, and Pan Hui. Edge Intelligence: Architectures, Challenges, and Applications. *arXiv:2003.12172*, 2020. [1](#)
- [38] Minjia Zhang and Yuxiong He. Accelerating Training of Transformer-Based Language Models with Progressive Layer Dropping. In *NeurIPS*, 2020. [4](#), [8](#)
- [39] Yuqing Zhao, Divya Saxena, and Jiannong Cao. Memory-Efficient Domain Incremental Learning for Internet of Things. In *SenSys*, 2023. [1](#)
- [40] Da-Wei Zhou, Qi-Wei Wang, Han-Jia Ye, and De-Chuan Zhan. A Model or 603 Exemplars: Towards Memory-Efficient Class-Incremental Learning. In *ICLR*, 2023. [2](#), [6](#)